INERTIAL CLUSTERING OF DROPLETS IN HIGH-REYNOLDS-NUMBER LABORATORY TURBULENCE

Ewe Wei Saw[1], Raymond A. Shaw[1]*, Sathya Ayyalasomayajula[2], Patrick Y. Chuang,[3] Armann Gylfason[2], and Zellman Warhaft[2]

[1]Dept. of Physics, Michigan Technological Univ., Houghton, MI, USA
[2]Mechanical and Aerospace Engineering, Cornell Univ., Ithaca, NY, USA
[3]Dept. of Earth Sciences, Univ. of California Santa Cruz, Santa Cruz, CA, USA

1. Motivation

Clustering of droplets in cloud due to turbulence is believed to have important consequences for warm rain formation (1), yet a detailed understanding is still lacking. To study the dependence of inertial particle clustering on turbulence parameters we have investigated the spatial distribution of particles in laboratory turbulence. The laboratory has the advantage of allowing user-control of turbulent flow and droplet properties, and it provides statistically stationary turbulence where robust, long-time averaging can be accomplished. The facility used is unique in providing nearly-homogeneous, isotropic turbulence, at Reynolds numbers approaching geophysical Reynolds numbers.

Physically, inertial clustering can be understood as the result of particles being centrifuged out of turbulent vortices and thus congregating in regions of high strain (2; 3; 4). The clustering is therefore significant at dissipation scales and below because it is in this range that turbulent vorticity and accelerations are strongest (5; 6). It should be noted, however, that alternate interpretations and approaches exist (7; 8; 9), adding impetus to the need for experimental data capable of elucidating mechanisms and constraining theory. To that end, it is the purpose of this letter to describe an experimental study of inertial clustering and its dependence on particle size and turbulence conditions.

*Corresponding author: rashaw@mtu.edu

Suitable quantification of clustering is provided by the particle pair correlation function $\eta(r)$ (4; 10), whose magnitude characterizes the strength of clustering at scale r. Intuition on the properties of $\eta(r)$ can be gain by examining how it is calculated from experiment:

$$\eta(r) = \frac{\langle \rho_p(r) \rangle}{\rho_p} - 1 \tag{1}$$

where $\langle \rho_p(r) \rangle$ is the particle density at distance r relative to each particle averaged over all particles; ρ_p is the global particle density. Previous studies (6; 11; 12), suggest that under ideal conditions (homogenous and isotropic turbulence, single-size particle population, particle-fluid coupling following Stokes's law, dilute particle loading, and negligible role of gravity) $\eta(r)$ satisfies a simple power law:

$$\eta(r) \propto (r/r_k)^{-f(St)} \tag{2}$$

where r_k is the Kolmogorov length scale (loosely, the size of the smallest turbulent eddies), $f(St) > 0$ and increases monotonically with St, the Stokes number, which characterizes the particle inertia. In this context, St is the ratio of the particle inertial response time τ_d to the Kolmogorov time τ_k (coherence time scale for the smallest eddies) (13):

$$St = \frac{\tau_d}{\tau_k} = \frac{1}{18}\left(\frac{\rho_d}{\rho}\right)\left(\frac{d}{r_k}\right)^2, \tag{3}$$

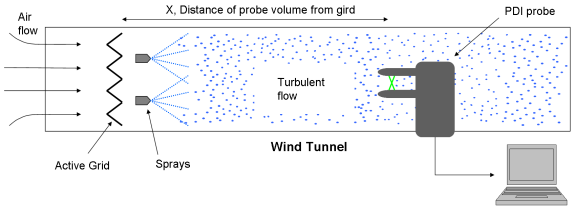

Figure 1: Experimental setup, including wind tunnel with active grid, spray nozzles, and the phase Doppler interferometer for measuring droplet arrival time, size, and longitudinal speed.

where ρ_d is the droplet mass density, d is the droplet diameter, and the Kolmogorov microscale $r_k = (\nu^3/\varepsilon)$ depends on the kinematic viscosity ν of the fluid (air) and the turbulent kinetic energy dissipation rate ε.

2. Experiment Description

The experimental setup, shown in Fig. 1, consists of a wind tunnel with well-characterized turbulence, sprays for particle generation, and a particle detector. Homogenous and nearly isotropic turbulent flow is generated by a motorized 'active grid' capable of achieving Taylor-scale Reynolds number (R_λ) as high as 750. Detailed description of the wind tunnel and active grid can be found in (14). Water droplets are introduced via four spray nozzles, with the resulting size distribution being quite broad ($\bar{d} = 22\ \mu$m, $\sigma_d = 13\ \mu$m). Downstream, a Phase Doppler Interferometer (PDI) (15) simultaneously measures the diameter (d_i), downstream speed (v_i), and arrival time (t_i) of any droplets that traverse its view volume (which has a linear dimension of roughly $150\ \mu$m). The PDI system was built and calibrated by Artium Technologies, Inc. and is designed for *in situ* measurement, such that the instrument does not disturb the flow through the measurement volume when aligned parallel to the mean flow. To characterize the turbulence, the wind tunnel and active grid are run with the sprays off, and air velocity statistics are measured with a hot-wire anemometer (HWA). The results of these 'dry' measurements are applicable to the experiments with droplets because of the small liquid-to-air volume ratio ($< 2.3 \times 10^{-5}$) and mass ratio ($< 4.8 \times 10^{-2}$), where flow modulation by the droplets is negligible (16). Comparison of velocity statistics obtained by PDI and HWA under identical flow conditions confirm this assumption.

Table 1: Experiment flow parameters.

Experiment	3m20Hz	3m30Hz	5m20Hz	5m30Hz
R_λ	515	664	443	590
ε (m^2s^{-3})	1.56	5.36	0.556	2.01
U (ms^{-1})	4.69	6.78	4.59	6.81
u (ms^{-1})	0.80	1.23	0.57	0.91
r_k (μm)	210	154	272	197

The PDI probe is stationed far enough downstream ($X = 3$ and 5 m) such that the droplets (except the largest drops, which are not included in this study) have ample interaction time with the turbulence to achieve equilibrium dynamics. This follows from the fact that the transit time of droplets is much larger than Kolmogorov time scale (all results shown here are for $St \lesssim 1$ so τ_k is a conservative bound). For the largest drops with St sufficiently greater than unity, the above reasoning does not apply since such droplets tend not to respond to the smallest eddies because of their relatively short coherence time. The behavior of these large drops is still an open question, and future work will address the statistics of $St \gg 1$ particles, and the time required for such particles to lose memory of their initial conditions.

To obtain the droplet spatial distribution (x_i) needed for the evaluation of $\eta(r)$ (using equation (1)), we adopt 'Taylor's hypothesis' (13) which states that when there is large mean flow, the small-scale features of the turbulence experience negligible evolution as they are advected passed a fixed measurement point. For our purposes, this translates to $x_i = t_i U$, with $U \equiv \overline{v_i}$ being the mean speed of the flow (note that errors resulting from the use of Taylor's hypothesis are negligible compared to uncertainties due to counting statistics, to be discussed later). Table 1 lists the flow parameters of the various experiments carried out in the wind tunnel: the experiments differ in R_λ and ε, and therefore have different r_k. Each experiment is referred to by a name based on the distance downstream from the active grid (in meters) where measurements are taken and the speed of the fan (in Hz) that drives the wind tunnel. Within each experi-

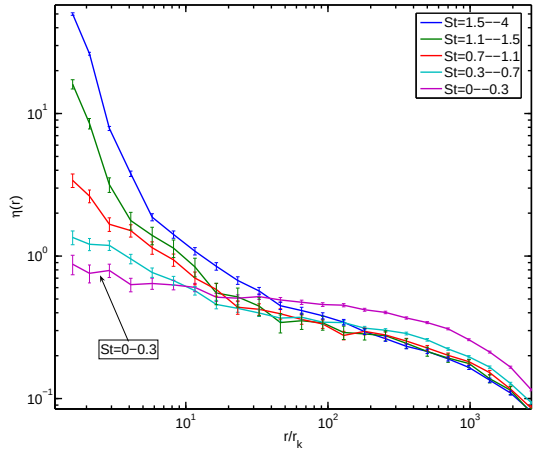

Figure 2: (color online) $\eta(r)$ versus $\hat{r}\,(\equiv r/r_k)$ with error bars of $2\sigma_{\eta(r)}$, and with $\eta(r)$ parameterized by St from experiment 3m30Hz. Each line is $\eta(r)$ calculated from droplets within a particular St range with the order from bottom to top corresponding to successively larger St.

ment, the dependence of clustering on particle inertia is studied by selecting droplets conditioned on their Stokes number St and then evaluating $\eta(r)$ for that subset of droplets. In practice, a range of Stokes numbers is used such that acceptable counting statistics are obtained.

3. Inertial Clustering Results

The essential experimental results on particle clustering are presented in Figs. 2 and 3, which depict the dependence of $\eta(r)$ on $\hat{r} \equiv r/r_k$ for various flow conditions; Note that in light of Eq. 2 the data are plotted on a log-log scale. Fig. 2 illustrates how $\eta(r)$ changes with St within a single experiment (3m30Hz). We note that strong clustering is mainly limited to scales $\hat{r} \lesssim 30$ and that clustering is stronger for droplets of larger St. Onset of clustering in the dissipation subrange, and monotonic increase of clustering with St is consistent with theories valid for $St < 1$ (6; 11). In the inertial subrange, $50 \lesssim \hat{r} \lesssim 300$, the correlation functions tend to a plateau signifying relatively weak clustering, and then fall off again at larger $\hat{r}$. This inertial-subrange behavior typifies correlations arising from mixing of a passive scalar by turbulence (e.g., correlation function scaling as $1-(r/l)^{2/3}$ (17)). Essentially, mixing progresses from large-scale inhomogeneities in the droplet spatial distribution induced by the spray injection that are subsequently stretched and distorted in the turbulent cascade, as the droplets are advected downstream. Consequently, we expect and observe (not shown here) that this plateau region is lower in magnitude for experiments with $X = 5$ m, where the mixing is more complete, relative to $X = 3$ m. Finally, while this study is focussed on $St \lesssim 1$, a curve for $1.1 < St < 4$ is included in panel a) to illustrate an intriguing possibility: It can be seen that the onset of inertial clustering (signified by the sudden change in slope near the dissipation range) occurs at larger $\hat{r}$ for $St > 1$. This hints at the possibility that droplets with $St > 1$ may exhibit strong inertial clustering, contrary to computational and theoretical findings (9; 12), and experiments at low Reynolds numbers (18). A possible reason is that the particles tend to form clusters of larger size, induced by inertial-subrange eddies of size a for which $St_a = \tau_d/\tau_a \approx 1$ is satisfied. Note that a similar phenomenon has been observed in simulations of two-dimensional turbulence (7). This phenomenon is unlikely to be appreciable in turbulence simulations and experiments with relatively low Reynolds numbers and, consequently, a limited range of scales in the inertial subrange (given that $R_\lambda \sim (l/r_k)^{2/3}$).

The uncertainty in $\eta(r)$ is estimated by assuming Poisson statistics for counting of droplets in the range $[r, r+\triangle r]$ relative to each droplet. This yields $\sigma_{\eta(r)} = \sqrt{\langle \eta(r)+1 \rangle / N \rho_p \triangle r}$, where N is the total number of droplets present. $\langle . \rangle$ signifies ensemble average, but the calculated value of $\eta(r)$ is used as an estimator for this purpose. Other sources of error are negligible compared to this counting uncertainty, as discussed earlier. We also note that these measurements were made in one spatial dimension, but inertial clustering is inherently three dimensional. It has been shown that the resulting spatial averaging can suppress the true clustering signature (19), but this is not a significant problem in these experiments because the averaging scale is always less than the correlation scale r.

Droplets with different diameters but equal Stokes numbers from the various experiments are compared in

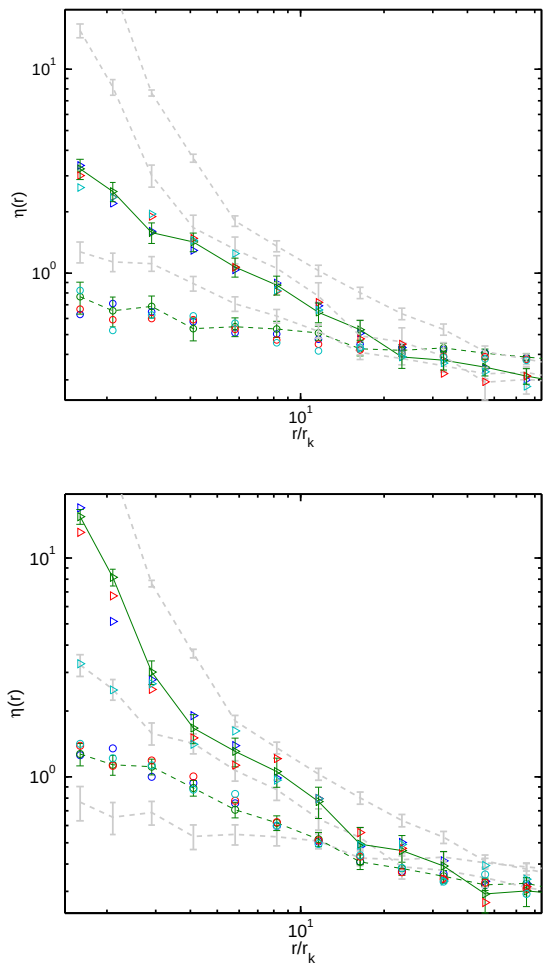

Figure 3: (color online) Stokes-similarity results shown in two panels for clarity. **a)** St-similarity for droplets with St=0-0.4 (circles) and St=0.7-1.1 (triangles). Plots for other St groups from Fig. 2, 3m30Hz, are shown in the background for comparison. The marker colors represent $\eta(r)$ from different experiments (blue=3m20Hz, green=3m30Hz, red=5m20Hz, cyan=5m30Hz). **b)** St-similarity for St=0.4-0.7 (circles) and St=1.1.-1.4 (triangles).

Fig. 3, demonstrating 'Stokes similarity' as expected from scaling arguments for inertial clustering. The $\eta(r)$ values for the same St range coincide to within the experimental error even though each is obtained from different flow conditions and droplet sizes. This is, to the knowledge of the authors, the first experimental report of such St-similarity in turbulence. The plots in Fig. 3 are obtained by re-normalizing each $\eta(r)$ such that they coincide in the inertial subrange (the plateau region). Conceptually, the fine-scale correlations due to droplet inertia are 'superimposed' on the larger-scale correlations resulting from traditional turbulent (scalar) mixing — and therefore comparison of fine-scale features requires that the large scales first be matched. Large-scale correlations, to first order, lead to a multiplicative constant on the magnitude of $\eta(r)$ for r smaller than the correlation scale, thus the re-normalization is achieved by multiplying a constant factor to each $\eta(r)$. The effect is most pronounced when comparing results from 3 m and 5 m because the latter has mixed more thoroughly. For example, we found that $\eta(r)$ curves corresponding to 5 m are consistently diminished by a constant factor from their 3 m counterparts. Similar variations are also observed among some experiments at the same X due to other variabilities in the injecting sprays and the mixing process.

In some experiments we observe signs of departure from Stokes similarity, as evident in panel b) for one set of triangular markers for $0.7 < St < 1.1$. For that set of experimental conditions we find that $\eta(r)$ has significantly lower values at the smallest scale resolvable by our instrument, as compared to the other experiments with the same St range. Although the data with $St > 1$ are prone to uncertainties in counting statistics and the question of droplet equilibration, we find that Stokes similarity is less robust for $St > 1$. This phenomenon is a focal point of future experiments.

An important observation from Fig. 3 is the apparent power-law dependence of $\eta(r)$ on spatial scale $\hat{r}$. As discussed in the introductory section, this is consistent with theoretical expectations for $St \lesssim 1$ (see Eqtn. 2). Within the limited resolvable scales, the correlation functions appear to be linear on the log-log scale, with slope increasing monotonically with St, also qualitatively consistent with theory (6; 11). (For $St \gtrsim 1$ there is an apparent change in slope near $\hat{r} \approx 3$ that suggests deviation from the $St \lesssim 1$ theory.) Quantitative comparison between the

experimental results and computational and theoretical findings is troublesome because idealized studies treat all droplets as having the same St. In real experiments narrow size bins are very difficult to achieve with reasonable counting statistics, and therefore broad St ranges must be used. However, when the data presented in Figs. 2 and 3 are processed with progressively narrower St bins (not shown here), an unambiguous increase in the magnitude of $\eta(r)$ at fine scales is observed. Indeed, this observation is further evidence that the fine-scale clustering is due to droplet inertia: theory suggests that droplets respond to the turbulent flow such that the maximum spatial correlation is between droplets of identical St. For droplets with different St the power-law exponent is reduced, and when the difference is too large the power-law dependence is lost altogether. A goal of subsequent experiments, therefore, will be to close this gap between theory and experiment, at least in part by increasing counting statistics.

The experiments described here provide strong support for the inertial clustering mechanism, and are in qualitative agreement with theoretical predictions. Briefly, clustering distinct from that expected for a passive scalar constituent is observed at dissipative scales, where fluid acceleration and vorticity reach a maximum. The magnitude of the clustering increases monotonically with droplet St, which characterizes coupling between the particles and the fluid. Finally, under distinct flow conditions and with varying droplet sizes, the dissipation-range clustering is observed to exhibit Stokes similarity. These experimental results lead naturally to several additional aspects of the problem that will require additional measurements and analysis. We conclude with a brief discussion of problems for future work. Much remains to be studies regarding the behavior of drops with $St > 1$, and this will require improved counting statistics to reduce counting uncertainties, and a thorough investigation of drop equilibration times. The effects of gravity have not been considered here because of the large ε for all flows; but as the energy dissipation rate is decreased, a second dimensionless parameter, the ratio of Kolmogorov and gravitational settling speeds, is expected to play a role. The dependence of inertial clustering on turbulence Reynolds number is an open question (20), and has important implications for geophysical problems; improved counting statistics and additional experiments should allow for further investigation of possible dependence on Re_λ.

Acknowledgement This work was supported by the U.S. National Science Foundation (grant ATM-0320953) and by the Max Planck Institute for Dynamics and Self-Organization. We are indebted to E. Bodenschatz, L. R. Collins, J. P. Fugal, A. B. Kostinski, D. Lamb, and M. Larsen for insightful comments and suggestions. We thank J. Small, W. Bachalo and the staff at Artium Technologies for technical assistance with the PDI instrument.

References

[1] M. Pinsky and A. Khain, Quart. J. Roy. Meteor. Soc. **123**, 165 (1997).

[2] M. R. Maxey, J. Fluid Mech. **174**, 441 (1987).

[3] J. K. Eaton and J. R. Fessler, Int. J. Multiphase Flow **20**, 169 (1994).

[4] S. Sundaram and L. R. Collins, J. Fluid Mech. **335**, 75 (1997).

[5] L. P. Wang and M. R. Maxey, J. Fluid Mech. **256**, 27 (1993).

[6] J. Chun, D. L. Koch, S. L. Rani, A. Ahluwalia, and L. R. Collins *et al.*, J. Fluid Mech. **536**, 219 (2005).

[7] L. Chen, S. Goto, and J. C. Vassilicos, J. Fluid Mech. **553**, 143 (2006).

[8] K. Duncan, B. Mehlig, S. Östlund, and M. Wilkinson, Phys. Rev. Lett. **95**, 240602 (2005).

[9] L. I. Zaichik and V. M. Alipchenkov, Phys. Fluids **15**, 1776 (2003).

[10] R. A. Shaw, Ann. Rev. Fluid Mech. **35**, 183 (2003).

[11] G. Falkovich, A. Fouxon, and M. G. Stepanov, Nature **419**, 151 (2002).

[12] W. C. Reade and L. R. Collins, Phys. Fluids **12**, no. 10, 2530 (2000).

[13] H. Tennekes and J. L. Lumley, *A First Course in Turbulence*, (MIT Press, Cambridge, MA, 1972).

[14] L. Mydlarski and Z. Warhaft, J. Fluid Mech. **320**, 331 (1996).

[15] W. D. Bachalo and S. V. Sankar, in *CRC Handbook of Fluid Dynamics*, (CRC Press, 1996).

[16] S. Geiss, A. Dreizler, Z. Stojanovic, M. Chrigui, A. Sadki, and J. Janicka, Exp. Fluids **36**, 344 (2004).

[17] J. Abrahamson, Chem. Eng. Sci. **30**, 1371 (1975).

[18] A. M. Wood, W. Hwang, and J. K. Eaton, Int. J. Multiphase Flow **31**, 1220 (2005).

[19] G. L. Holtzer and L. R. Collins, J. Fluid Mech. **459**, 93 (2002).

[20] L. R. Collins and A. Keswani, New J. Phys. **6**, 119 (2004).